The 6.5-day wave and its seasonal variability in the middle and upper atmosphere

H.-L. Liu,[1] E. R. Talaat,[2] R. G. Roble,[1] R. S. Lieberman,[3] D. M. Riggin,[3] and J.-H. Yee[2]

Received 19 March 2004; revised 6 June 2004; accepted 2 August 2004; published 12 November 2004.

[1] The zonal wave number 1 planetary wave of period near 6.5 days is a robust feature in the mesosphere and lower thermosphere (MLT) region with prominent seasonal variability as revealed by ground based and satellite observations. This wave and its seasonal variability are well reproduced in a recent one model year run of the National Center for Atmospheric Research thermosphere-ionosphere-mesosphere-electrodynamics general circulation model (TIME-GCM) with its lower boundary specified according to the National Centers for Environmental Prediction analysis (year 1993). Wavelet analysis of the model output shows that in the MLT region the wave maximizes before and after the equinoxes and minimizes at solstices. The wave amplitudes at the equinoxes are smaller than the peaks before and after but are still larger than the wave amplitudes at solstices. However, at the lower boundary near 30 km the wave peaks are predominantly between fall and the following spring. By examining the episodes of maximum and minimum wave amplitude and by conducting additional control experiments using the TIME-GCM, the structure of this planetary wave and the factors determining the wave characteristics and seasonal variability are studied in detail. It is found that the wave source, mean wind structure, instability, and the critical layers of the wave can all affect the wave response in the MLT region and can have a strong seasonal dependence. Before and after equinox, the wave follows the waveguide and propagates from the stratosphere to the summer mesosphere/mesopause, where it may amplify due to baroclinic/barotropic instability. Such instability is usually absent from the equinoctial atmosphere, so that there is no wave amplification at equinox. At solstice the wave decays significantly when propagating away from its winter source due to the strong eastward winter stratospheric jet. In the summer side the westward jet is also strong, and the meridional and vertical extension of the critical layer of the wave is large enough to enclose the instability in the summer mesosphere/mesopause at middle to high latitudes. The wave is thus reflected away and prevented from reaching and amplifying at the unstable region. The seasonal variation of the quasi-two-day wave, which has zonal phase speed similar to the 6.5-day wave, is also studied using similar diagnostics. It is further shown that within certain seasonal ''window'' periods, the variability in the MLT, especially the summer MLT, may closely track the lower atmospheric variability associated with these waves. *INDEX TERMS:* 3334 Meteorology and Atmospheric Dynamics: Middle atmosphere dynamics (0341, 0342); 3332 Meteorology and Atmospheric Dynamics: Mesospheric dynamics; 3384 Meteorology and Atmospheric Dynamics: Waves and tides; *KEYWORDS:* planetary wave, 6.5-day wave, 2-day wave, mesosphere, variability

Citation: Liu, H.-L., E. R. Talaat, R. G. Roble, R. S. Lieberman, D. M. Riggin, and J.-H. Yee (2004), The 6.5-day wave and its seasonal variability in the middle and upper atmosphere, *J. Geophys. Res.*, *109*, D21112, doi:10.1029/2004JD004795.

1. Introduction

[2] Westward propagating planetary wave with 5–7 day period and wave number 1 is a robust feature in the middle and upper atmosphere, and has been identified by both ground based and satellite observations [*Hirota and Hirooka*, 1984; *Wu et al.*, 1994; *Riggin et al.*, 1997; *Talaat et al.*, 2001, 2002; *Lieberman et al.*, 2003]. It was first suggested [*Wu et al.*, 1994] that the wave may correspond to the free Rossby (1,1) mode, the 5-day wave [*Madden and Julian*, 1972], with a longer wave period due to Doppler shift by atmospheric winds. *Meyer and Forbes* [1997] argued that the actual wave period in a 1993 strong wave event is 6–7 days, while the change of the 5-day wave period due to Doppler shift would be less than 0.5 day [*Geisler and Dickinson*, 1976]. They instead demonstrated that the me-

[1]High Altitude Observatory, National Center for Atmospheric Research, Boulder, Colorado, USA.
[2]Applied Physics Laboratory, Johns Hopkins University, Laurel, Maryland, USA.
[3]Colorado Research Associates, Boulder, Colorado, USA.

0148-0227/04/2004JD004795

sosphere at middle and high latitudes could be baroclinically/barotropically unstable before equinox (1 September), and that the instability could act as an in situ wave source for the planetary wave. They were able to determine that the westward zonal wave number 1 wave response to a mesosphere in situ momentum source peaks at 6.5-day period, by using the Global Scale Wave Model (GSWM) [*Hagan et al.*, 1995]. This theory is supported by recent analysis by *Lieberman et al.* [2003].

[3] *Talaat et al.* [2001] showed that the 6.5-day wave perturbation of the horizontal winds, temperature, and nighttime atomic oxygen emissions at 95 km, derived from HRDI observations, all display latitudinal structures similar to the gravest symmetric wave number 1 Rossby (1,1) mode. The vertical amplitude and phase structures of the wave, on the other hand, indicates that it is an internal Rossby wave, rather than an external Lamb wave. *Talaat et al.* [2002] further strengthened this point, by combining the UKMO stratospheric data and HRDI mesospheric and lower thermospheric data and demonstrating the phase and amplitude consistency of the wave from the stratosphere to the lower thermosphere. Such consistency, they suggested, indicates the vertical propagation of the wave from the stratosphere to the mesosphere and lower thermosphere (MLT).

[4] Seasonal variation of the 6.5-day wave is also clear from the observations [*Talaat et al.*, 2001, 2002; *Lieberman et al.*, 2003], with the maximum wave amplitude near equinox. The large wave event modeled by *Meyer and Forbes* [1997] was also within a month before the September equinox. *Talaat et al.* [2001, 2002] further showed that the 6.5-day wave at mesospheric altitudes peaks before and after the 1994 September equinox, and the associated wind perturbation near the equator is biased toward the summer hemisphere (i.e., Northern Hemisphere before the September equinox and Southern Hemisphere afterward). This indicates that the wave propagation is likely to be dependent on the atmospheric winds. It also implies that the wave amplification may not be solely determined by the atmospheric stability: Baroclinic/barotropic instability is more likely to be present and stronger in the mesosphere at solstice than around equinox due to larger wind shear, but the wave is generally weak around solstice.

[5] In this study, we will study the factors that determine the propagation and amplification of the 6.5-day wave and how these factors change with season. The numerical model employed for this study is the National Center for Atmospheric Research thermosphere-ionosphere-mesosphere-electrodynamics general circulation model (NCAR TIME-GCM), and in this simulation daily values of the National Centers for Environmental Prediction (NCEP) reanalysis are specified as its lower boundary at 10 hPa. By examining the TIME-GCM 1993 simulation results, it is found that the 6.5-day wave displays seasonal variations similar to those found by *Talaat et al.* [2001, 2002], and *Lieberman et al.* [2003]. In this study, we will analyze these simulation results, as well as auxiliary control model simulations, to elucidate the processes of the wave propagation and amplification under different seasonal conditions. We will demonstrate that the wave response in the MLT is closely tied to the waveguide, the critical layer, and the baroclinic/barotropic instability. We will also examine the seasonal variation of the quasi two-day wave, which has phase speed roughly equal to that of the 6.5-day wave, using the same diagnostics and show the similarity and difference in their respective seasonal variations.

2. Numerical Experiments

[6] The 1993 TIME-GCM simulation was described in details by *Walterscheid et al.* [2000] and *Hagan and Roble* [2001]. We will only highlight some important aspects of the model and the simulation here. TIME-GCM is the latest in a series of three-dimensional time-dependent models that have been developed over the past two decades to simulate the circulation, temperature, and compositional structure from the upper stratosphere to the thermosphere. It combines all the previous features of the TGCM [*Dickinson et al.*, 1981, 1984], TIGCM [*Roble et al.*, 1988], and TIE-GCM [*Richmond et al.*, 1992]. It includes aeronomical processes appropriate for the mesosphere and upper stratosphere, as described by *Roble and Ridley* [1994], *Roble et al.* [1987] and *Roble* [1995]. The model is a grid point model with fourth-order horizontal differencing on a $5^\circ \times 5^\circ$ latitude/longitude grid. The version used in this simulation has 45 pressure surfaces extending from 10 hPa (about 30 km height) to above 500 km with a vertical resolution of 2 grid points per scale height and a model time step of 5 min. Leapfrog scheme is used for time integration of advection and implicit scheme is used for vertical diffusion. Details of the numerical framework of the model can be found in the work of *Dickinson et al.* [1981]. Diurnal and semidiurnal tidal components due to tropospheric forcing are specified at the lower boundary from the Global Scale Wave Model (GSWM) [*Hagan et al.*, 1999]. The gravity wave effects in TIME-GCM need to be parameterized and the parameterization is based on linear saturation theory by *Lindzen* [1981]. In the 1993 simulation, the NCEP reanalysis daily data are specified at the lower boundary of the TIME-GCM, and the model is able to resolve the upward propagation of those realistic perturbations resolvable by the NCEP data. In addition to this whole year simulation, auxiliary numerical experiments were also conducted for control studies. In these control cases, the lower boundary forcing by NCEP is replaced by idealized planetary wave perturbations with specific wave amplitudes and periods.

3. Analysis of Model Results

[7] We first run the TIME-GCM simulation results through a spectral analysis to identify the planetary waves and their variation in this model year. In this study our primary concern is the wave number 1 wave with period around 6.5 days. Hence a forward and a reverse FFT are first applied in the longitutinal direction to a specific field variable (e.g., zonal wind) for each model day at 0 UT to obtain its wave number 1 component. This field variable with only wave number 1 is then processed by a continuous wavelet procedure [*Torrence and Compo*, 1998] in the temporal domain to identify dominant wave periods throughout the model year. Figure 1 shows the analysis result performed on the zonal wind at $\sim$93 km (0.0015 hPa) and 5 different latitudes corresponding to latitudes of the 5 radar sites used in the analysis by *Lieberman et al.* [2003]. It should be noted that the wave

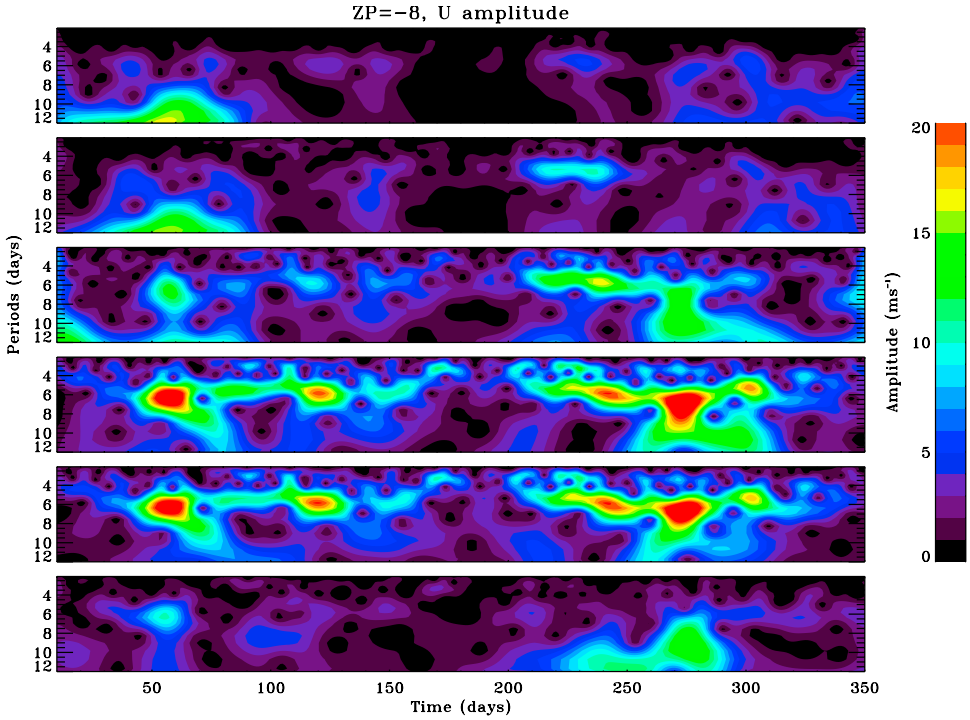

Figure 1. Wavelet analysis of the zonal wind wave number 1 component at 0.0015 hPa and (from the top) 52.5°N, 40°N, 22.5°N, 2.5°N, 7.5°S, and 35°S from the 1993 TIME-GCM simulation.

periods in this analysis are only for wave number 1, while those in the work of *Lieberman et al.* [2003] include all wave numbers. From Figure 1, wave number 1 components with period near 6.5 days maximize around both equinoxes and at low latitudes and are much weaker near solstice. This is in general agreement with the analysis of the radar data, though the latter displays larger wave amplitude around fall equinox.

[8] The temporal and spatial structures of the component with wave number 1 and period between 6–7 days can be examined by summing the wavelet powers in this period interval. The square root of this power (for zonal wind) as a function of time and latitude is shown in Figures 2a and 2b at ~93 km (0.0015 hPa) and ~30 km (10 hPa), respectively. The latter is the lower boundary of the TIME-GCM, and is thus also analysis results for NCEP data at 10 hPa. At 93 km and its maximum amplitude near both equinoxes, the latitudinal structure of the 6–7-day wave is quite symmetric with respect to the equator and consistent with that of the first symmetric mode of a Rossby wave with 6.5 days period [*Talaat et al.*, 2001]. However, this symmetry is not an exact one and the amplitude contour lines extending more toward the summer hemisphere (e.g., toward the Southern Hemisphere between day 50–60, and the Northern Hemisphere between day 220–250). Therefore the wave activity around equinox appears to shift from the pre-equinox summer hemisphere toward the postequinox summer hemisphere (i.e., northward around March equinox and southward around September equinox). Similar latitudinal shift has been identified for 6.5-day wave zonal wind amplitude around September equinox from the HRDI observation [*Talaat et al.*, 2002]. It can also be seen from Figure 2a that the amplitude subpeaks at high latitudes are also stronger in the summer hemisphere. At 10 hPa, on the other hand, the dominant wave activity is mainly in the winter hemisphere, especially at higher latitudes. Such seasonal variability and the difference between the mesosphere and the stratosphere can be better illustrated by examining the geopotential height perturbations (Figures 2c and 2d). The bias of the symmetric mode amplitude toward the summer hemisphere in the mesosphere and the dominant wave activity in the winter hemisphere in the stratosphere are unambiguously demonstrated in this plot.

[9] The model results thus capture the salient features of the observed 6.5-day wave and its seasonal variability. We now proceed to analyze the model results to understand the possible causes of the seasonal variability. Specifically, we will select time periods when the wave activity is strong (before and after equinox), moderate (at equinox), and weak (at solstice), and examine how the mean atmospheric state will affect the wave propagation at these times.

3.1. Seasonal Changes of the Mean State

[10] The propagation of planetary waves is closely related to the atmospheric mean state, such as zonal mean zonal wind and stratification. From the mean state, the refractive index m for a planetary wave with zonal wave number k and phase speed c can be calculated, under the quasi-geostrophic (QG) assumption, [e.g., *Andrews et al.*, 1987; *Salby*, 1997]

$$m^2 = \frac{\bar{q}_\phi}{a(\bar{u}-c)} - k^2 - \frac{f^2}{4N^2H^2}, \qquad (1)$$

where a, ϕ, f, N, and H are the earth radius, latitude, Coriolis parameter, Brunt-Väisällä frequency, and pressure scale

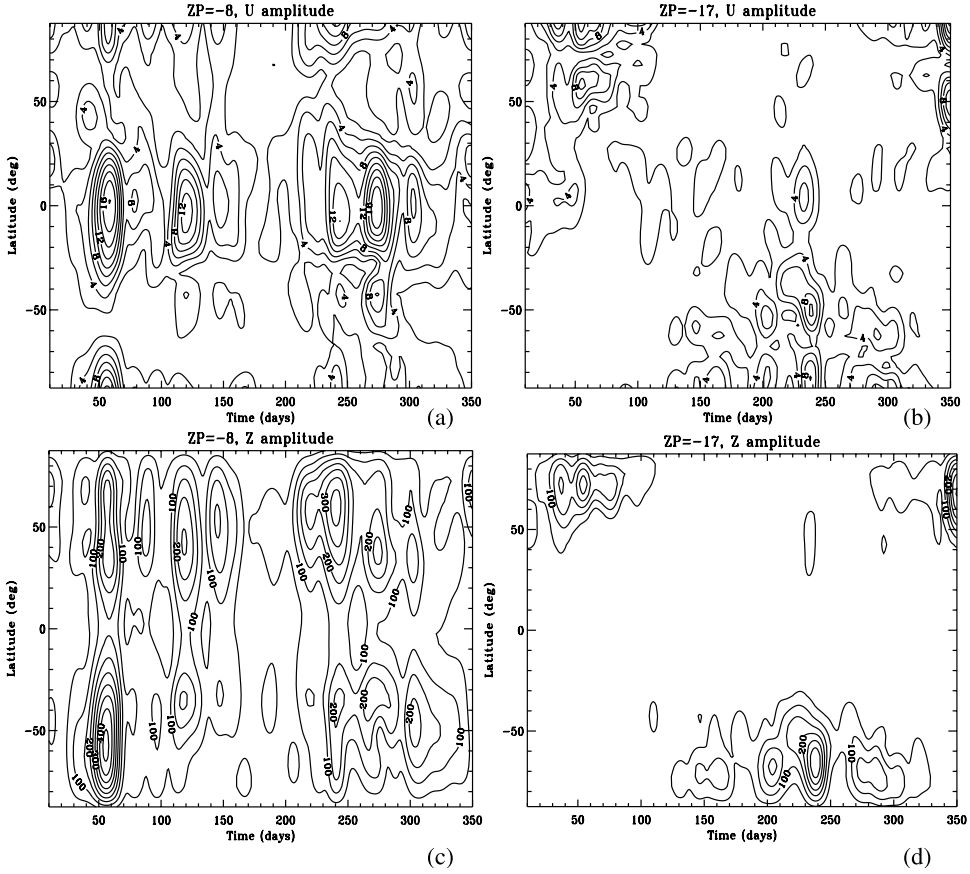

Figure 2. Square root of the total power of zonal wind wave number 1 component between 6 and 7 days period from the wavelet analysis at (a) 0.0015 and (b) 10 hPa levels. (c and d) Similar to Figures 2a and 2b, but for geopotential height (in meters).

height, respectively. $\bar{u}$ is the zonal mean zonal wind, and $\bar{q}_\phi$ is the latitudinal gradient of the QG potential vorticity

$$\bar{q}_\phi = 2\Omega\cos\phi - \left(\frac{(\bar{u}\cos\phi)_\phi}{a\cos\phi}\right)_\phi - \frac{a}{\rho}\left(\frac{f^2}{N^2}\rho\bar{u}_z\right)_z, \qquad (2)$$

where Ω is the angular speed of the earth rotation, and ρ is the air density. For a forced wave perturbation, the sign of the square of the refractive index m^2 reveals whether the wave is propagating or evanescent, and can thus be used as a proxy to the planetary waveguide. Planetary waves may also be affected by the instability of the atmosphere [*Meyer and Forbes*, 1997; *Limpasuvan et al.*, 2000]. A necessary condition for baroclinic/barotropic instability is $\bar{q}_\phi < 0$, and the criterion for inertial instability at the equator is

$$\mathcal{I} = f^2\left(1 - Ri^{-1}\right) - f\bar{u}_\phi/a < 0 \qquad (3)$$

[e.g., *Andrews et al.*, 1987]. We will examine how these quantities will vary with the season and how they may affect the wave propagation.

[11] Figure 3 shows these diagnostic quantities, as well as zonal mean zonal wind, over half of the annual cycle on days 10, 50, 80, 120, 150, and 180 calculated from the TIME-GCM/NCEP simulation. The shade at high latitudes indicates regions where $\bar{q}_\phi < 0$, while that near the equator highlights regions where $\mathcal{I} < 0$. m^2 is calculated assuming the wave period is 6.5 days and wave number is 1. m^2 is 0 at the thick contour lines at middle or high latitudes with m^2 positive on the equatorial side and negative on the polar side. The thick dash line indicates the critical layer for this wave.

[12] From these plots, it can be seen that $\bar{q}_\phi$ is negative at high latitudes in the summer mesosphere/mesopause below the reversal altitudes of the jet, due to the large positive curvature of the zonal wind in both meridional and vertical directions (equation (2)). The latitude-height cross section of the region with negative $\bar{q}_\phi$ shrinks and disappears from solstice to equinox due to the weakening of the jet and decrease of the wind curvatures (Figures 3a–3c), and then reappears and increases in the other hemisphere from equinox to solstice (Figures 3d–3f). On day 50 (Figure 3b), $\bar{q}_\phi$ also becomes negative in the winter mesosphere. This can be tied to the reversal of the polar jet due to a stratospheric warming event at that time. The latitude-height cross section of the region with negative $\mathcal{I}$ also maximize at solstice on the winter side of the equator (Figures 3a, 3e, and 3f), as a result of the large latitudinal shear of the wind near the equator (equation (3)). In the winter hemisphere and also in both hemispheres at equinox, the line of zero refractive index is between 30° and 50° latitudes. In the summer hemisphere, this line roughly follows the boundary of the negative $\bar{q}_\phi$ region and is located at much higher latitudes below and above this region, because of its smaller intrinsic phase speed $u - c$ and/or smaller positive value of

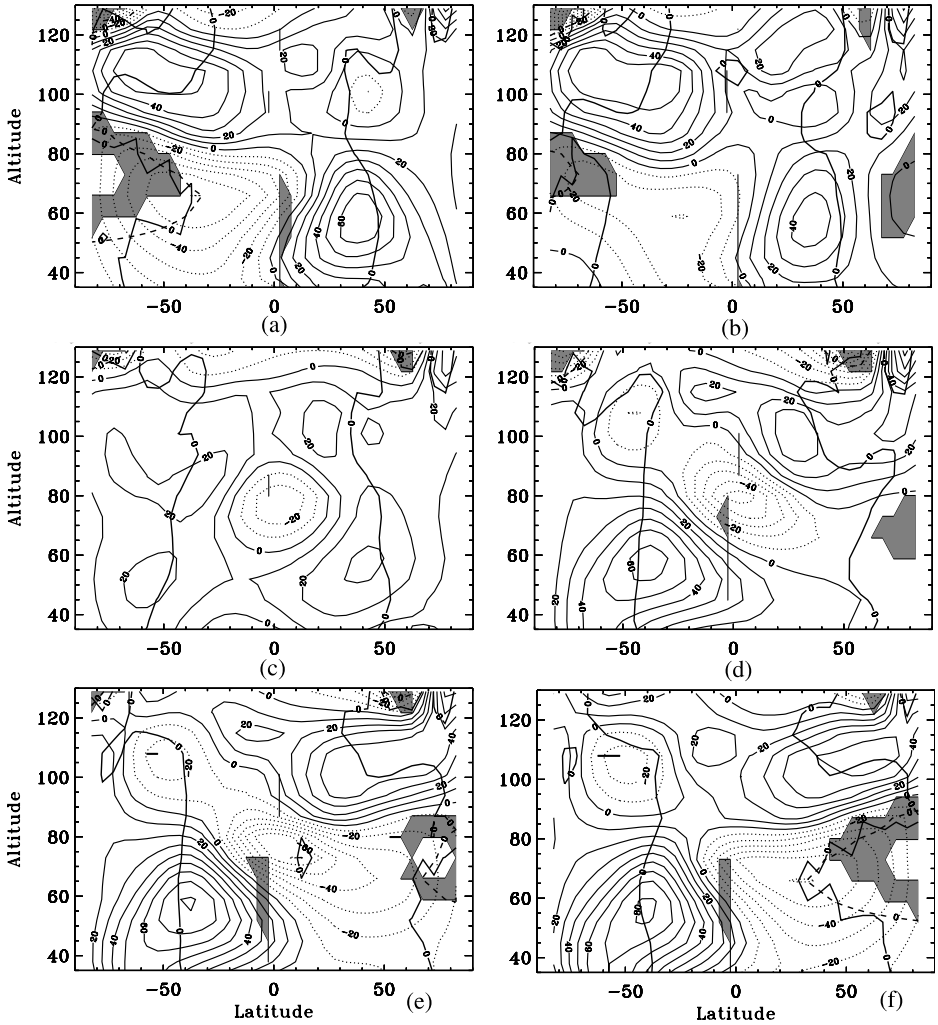

Figure 3. Zonal mean wind (thin contour lines, solid for eastward), zero refractive index lines (thick solid contour lines, with complex refractive indices poleward of these lines), critical layer for 6.5-day wave (thick dash contour lines), baroclinically/barotropically unstable region (shaded area at mid-high latitudes), and inertially unstable region (shaded area near equator) for days (a) 10, (b) 50, (c) 80, (d) 120, (e) 150, and (f) 180.

$\bar{q}_\phi$ (equation (1)). The critical layer of the wave extends from the polar region to midlatitudes at solstice in the summer mesosphere, and the region with negative $\bar{q}_\phi$ is almost completely enveloped within the critical layer (Figures 3a and 3f). As the westward wind decreases after solstice, the critical layer retreats to higher latitudes. On day 50, the critical layer is located inside the negative $\bar{q}_\phi$ region (Figure 3b). The critical layer disappears around equinox. In the following analysis, we will study how the wave characteristics can be related to these seasonal variations of the mean flow.

3.2. Seasonal Changes of the 6.5-Day Wave

[13] We examine and compare the wave characteristics at periods (1) after solstice and before equinox (henceforth loosely referred to as pre-equinox), (2) equinox, (3) after equinox and before solstice (referred to as postequinox), and (4) solstice. Specifically, the time periods of day 50–62, day 80–92, day 113–125, and day 200–212 are selected to highlight the episodes when the wave amplitude is high, moderate, high, and low (Figures 1 and 2). In the following analysis, we first focus on the comparisons between pre-equinox, equinox, and solstice, and then compare pre-equinox and postequinox episodes with the wave peaking at both. Figure 4 shows the 6.5-day wave amplitudes and phases of the zonal wind perturbations for these 3 periods. For the time period of day 50–62, the wave amplitude (Figure 4a) shows a clear vertical growth and latitudinal structure of a symmetric mode, though again with the amplitude on the summer side larger than the winter side in the mesosphere. There is a secondary peak near each polar mesopause, with the one on the summer side (11 ms^{-1}) larger than the one on the winter side (7 ms^{-1}). Both of these secondary peaks are located immediately above the negative $\bar{q}_\phi$ regions (Figure 3b). At the lower boundary near 30 km, the wave source is located in the winter hemisphere peaking between 40°N and 50°N. The phase flips between 30° and 40° (more clearly defined in the summer hemisphere)(Figure 4b), and it is consistent with the theoretical nodal point at ~37° of the Rossby (1,1) mode [*Talaat et al.*, 2002]. The apparent phase progression is downward on the equatorial sides of the nodal points and

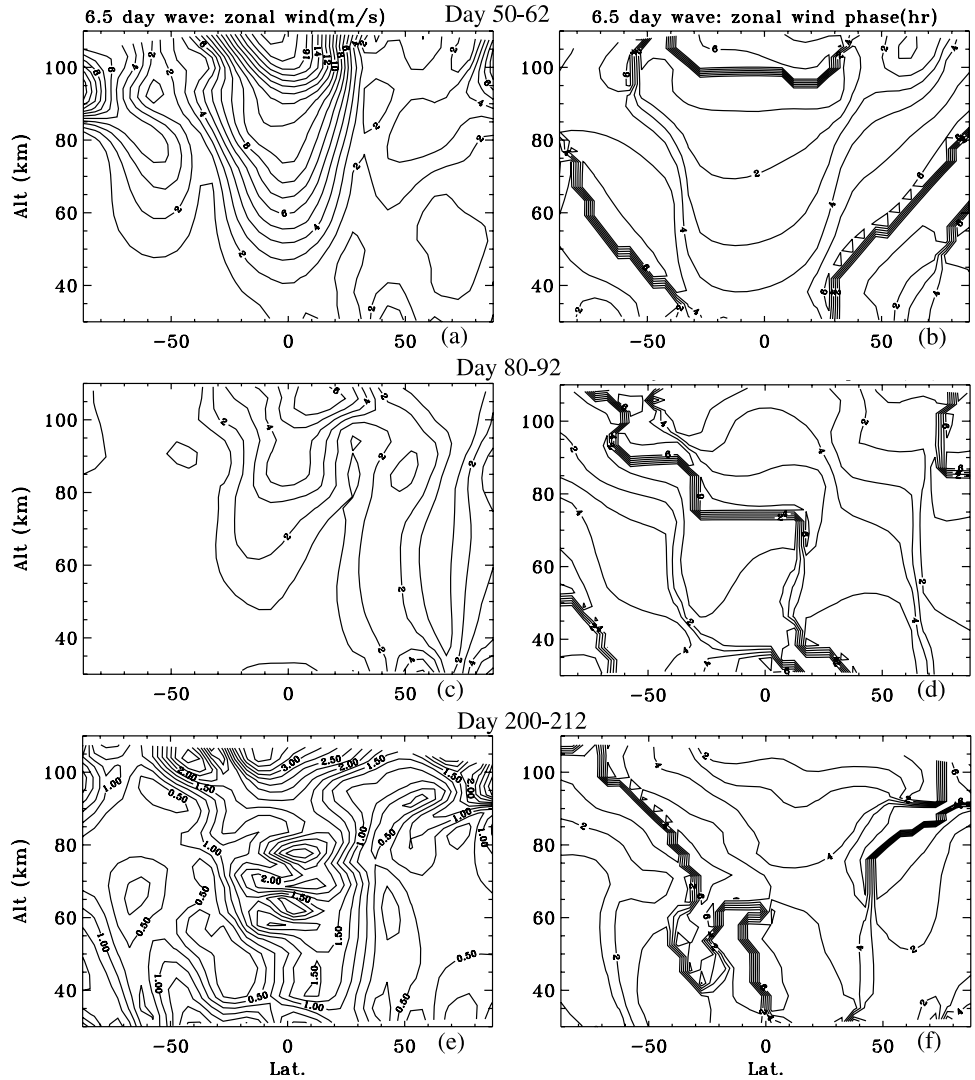

Figure 4. (left) The amplitude and (right) phase of 6.5-day wave zonal wind perturbations for the periods of (a and b) day 50–62, (c and d) day 80–92, and (e and f) day 200–212. The contour interval in Figures 4a–4d is 1 ms^{-1}, while it is 0.25 ms^{-1} in Figures 4e and 4f.

downward and poleward at higher latitudes (more clearly so in the winter hemisphere), consistent with the upward and equatorward energy flux from the wave source.

[14] At equinox (day 80–92), the 6.5-day wave amplitude is much smaller in the equatorial region and in the southern hemisphere (Figure 4c), with its peak equatorial amplitude less than one third of that during day 50–62. Zonal wind perturbation of the wave has almost disappeared in the southern hemisphere. In the northern hemisphere, the wave amplitude is smaller near the polar mesopause because the secondary peak has disappeared. The amplitude of the wave source (between 50°N and 60°N at 30 km) is actually larger than that at pre-equinox, but it barely grows with altitude. The latitudinal structure of the symmetric mode is still visible in the mesosphere, though the wave is mainly confined to the hemisphere with the wave source and thus the southern branch is much smaller than the northern branch. The nodes of the symmetric mode between 30° and 40° is visible in the phase plot (Figure 4d), but the phase progression is different. Poleward of the node in the northern hemisphere and above the wave source, the phase progression is mainly downward, which suggests that the wave does not propagate in the meridional direction as during the period of day 50–62. Equatorward of the nodes, the rate of the downward phase progression and also equivalently its westward tilt are much smaller in comparison with the pre-equinox case below 75 km.

[15] The wave amplitude at solstice (day 200–212) is insignificant in the mesosphere compared with those at the equinox and pre-equinox, even though the peak wave amplitude of the source is about half of that at pre-equinox. The wave amplitude around the equator in the mesosphere between 50 and 80 km shows spatial variation with small vertical scales (near the vertical grid size of the model). The vertical variation of the wave amplitude is reminiscent of the "pancake structures" and it coincides with the region with negative $\mathcal{I}$ region, and is thus likely caused by inertial instability [*Sassi et al.*, 1993, and references therein].

[16] The Eliassen-Palm (EP) flux and its divergence of the 6.5-day wave is shown in Figure 5 for these 3 time periods.

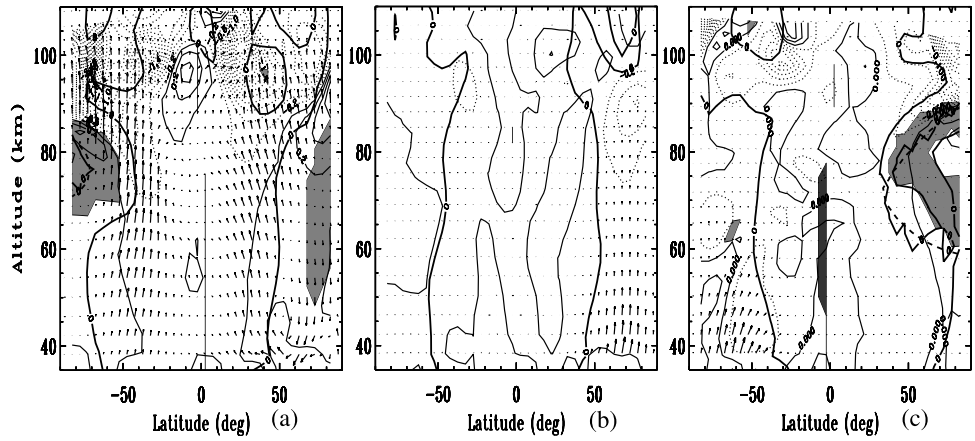

Figure 5. EP flux vectors and the divergence of the EP flux (thin contour lines, in the unit of $ms^{-1}d^{-1}$) of the 6.5-day wave, zero refractive index lines (thick solid contour lines), critical layer for 6.5-day wave (thick dash contour lines), and baroclinically/barotropically unstable region (shaded area at mid-high latitudes) for the periods of (a) day 50–62, (b) day 80–92, and (c) day 200–212.

For day 50–62 (Figure 5a), the upward EP flux of the wave is large in both hemispheres, especially at both polar mesopauses above where $\bar{q}_\phi$ is negative (again, the one in the northern hemisphere is due to stratospheric warming). The divergence of the EP flux is thus positive at these regions, indicating conversion to wave energy due to baroclinic or barotropic instability. The downward propagation of the wave energy from the unstable region can be clearly seen in the northern polar mesosphere and stratosphere. At equinox (Figure 5b), the overall EP flux is much weaker and decays considerably with altitude, which is consistent with the refractive index (Figure 3). At solstice (Figure 5c), the EP flux vectors generally point upward and from the source in the winter to the summer, with their magnitudes decreasing rapidly away from the source. A positive EP flux divergence appears above the negative $\bar{q}_\phi$ region, but the values are much smaller than those for the period of day 50–62 (notice that the contour interval in Figure 5c is about an order of magnitude smaller than in Figure 5a).

[17] To further elucidate the dependence of the 6.5-day wave on the atmospheric mean state at pre-equinox, equinox, and solstice, we perform 3 additional control TIME-GCM simulations. The lower boundary conditions in these simulations are not specified by the NCEP data, but rather by a prescribed wave perturbation with wave number 1 and 6.5 days periods so that the only planetary wave present is the 6.5-day wave. From Figure 2d it is seen that at 10 hPa the geopotential height perturbations of the wave can be found on both hemispheres but tend to be stronger at middle to high latitudes in the winter hemisphere. In the control simulations, the wave source is set only in one hemisphere: in the winter hemisphere for pre-equinox and solstice, and in the northern hemisphere for March equinox. The wave source is specified through geopotential height perturbation and it extends from 37.5° to the pole with its amplitude largest at 60°. In all three cases, the maximum geopotential height perturbation is set to the same value (50 m), so that the 6.5-day wave sources are identical and quantitative and direct comparisons can be made between the wave characteristics. The amplitude of the wave is set to a small value so that the wave is still approximately linear and the mean flow is not significant altered by the wave forcing. The mean atmospheric states in these runs are similar to but not exactly the same as those in the simulations with the NCEP boundary conditions.

[18] To enable more quantitative understanding and comparison of the wave behavior at different seasons, the meridional and vertical components of the EP flux (EPY and EPZ) of the 6.5-day wave are plotted separately. The EPY and EPZ from these 3 simulations are shown in Figure 6. It should be noted that the EPY and EPZ values shown in the plot have been normalized by the square root of the air density and EPZ has been multiplied by a scaling factor of 200 to make the values comparable to the EPY values. The contour interval value in the pre-equinox plots is twice as large as that in the equinox plots, which is another factor of 2 larger than that in the solstice plots. It is clear that both EPY and EPZ are the largest in the pre-equinox case, weakest under solstitial conditions, and moderate at equinox, even though the wave sources in the three cases are identical.

[19] Between solstice and equinox, the EP flux indicates that the major branch of the wave energy propagation roughly follows the waveguide crossing the equator and upward into the summer MLT. This explains the large upward EP flux in the southern hemisphere in Figure 5a, even though the wave source at the southern hemisphere lower boundary at this time is very weak. The simulation results also strongly suggest that the 6.5-day wave is over-reflected from the negative $\bar{q}_\phi$ region and amplify at the summer mesopause by converting mean flow energy to wave energy due to baroclinic/barotropic instability. The EPY of the reflected wave from that unstable region is obviously larger than the EPY of the incoming wave, so that the superposed EPY near that region is equatorward, opposite to the EPY of the incoming wave (Figure 6a). At the same time, EPZ is enhanced in the upper mesosphere and has a downward components below the unstable region (Figure 6b). The amplitudes of the 6.5-day wave are thus larger on the summer side, as seen in the observations and our numerical simulations.

[20] At equinox, the waveguide is mainly confined to the middle and low latitudes and there is no significant en-

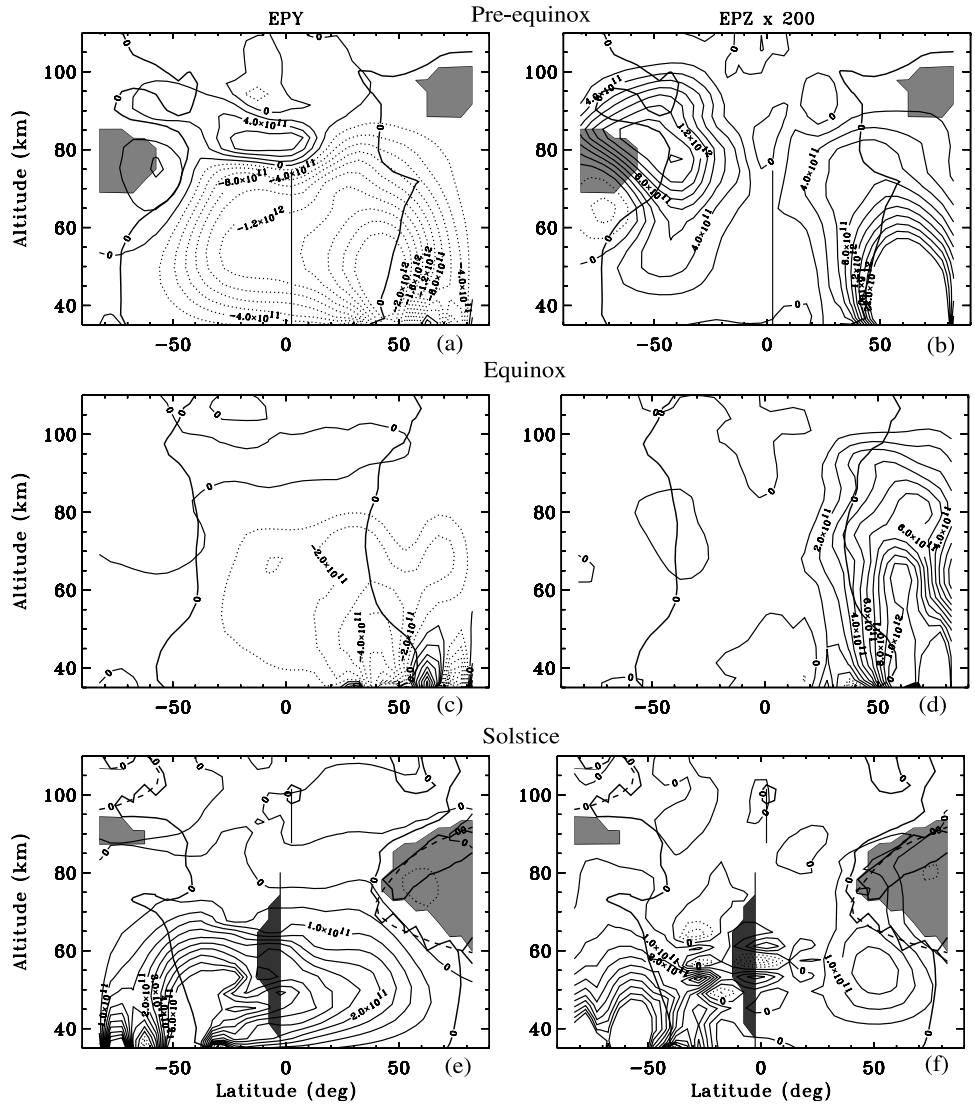

Figure 6. (left) Meridional and (right) vertical components of the EP flux of the 6.5-day wave in control simulations under (a and b) pre-equinoctial), (c and d) March equinoctial, and (e and f) June solstitial conditions. The solid contours are for northward or upward directions. Both components have been normalized by the square root of the air density (see text).

hancement due to instability. At the equator, EPY from the control simulation is about 10% of that in the pre-equinox case. EPZ is comparable with the pre-equinox case in the northern mesosphere but much smaller in the south. The wave amplitude is thus moderate in the northern hemisphere and very small in the south (Figure 4c). The zonal wind amplitude of the 6.5-day wave in the mesosphere at the equator is about 40% of the amplitude in the pre-equinox case.

[21] The EP flux from the control simulation of solstice has a relatively large cross-equatorial component compared with its vertical component (Figures 6e and 6f), but it is much smaller than the EPY in the pre-equinox case. At the equator, the maximum EPY at solstice near 50 km is about 30% of the pre-equinox value, and the ratio drops to about 10% at 30° in the summer hemisphere. EPY decreases to 0 near the critical layer, and there is no over-reflection. EPZ is also small in this case. At 60 km above the wave source, the EPZ at solstice is less than 10% of the pre-equinox value and decreases rapidly with altitudes. At the summer mesopause, there is no enhancement of EPZ above the negative $\bar{q}_\phi$ region, neither is there significant wave reflection (negative EPZ) below. The maximum zonal wind perturbation of the 6.5-day wave in the upper atmosphere is about 20% of the pre-equinox case.

[22] The small EP flux at solstice is most likely due to the strong eastward winter stratospheric jet [e.g., *Charney and Drazin*, 1961]. The jet near the wave source at 10 hPa is larger than 60 ms^{-1} and increases with altitudes, while in the pre-equinox case the jet near the wave source is about 20 ms^{-1}. It can be seen from equation (1) that larger values of $u - c$ will decrease m^2 so that the wave is more likely to be trapped and the decaying rate of the wave is larger if it is already trapped. In the summer mesosphere, the westward wind is also large, and the critical layer of the wave thus encompasses a large meridional and height range so that the

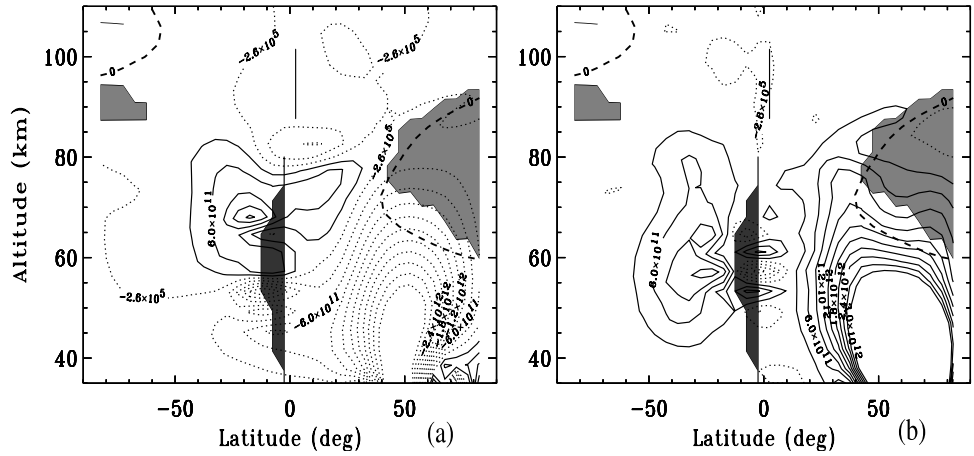

Figure 7. Similar to Figures 6e and 6f, but the wave source is now moved to the summer hemisphere.

negative $\bar{q}_\phi$ region is mostly enveloped within the critical layer (Figures 6e, 6f, 3a, and 3f). The critical layer, therefore, acts as a "shield" around the unstable region by preventing the wave from reaching and over-reflecting from that region. Figures 6e and 6f also show that inertial instability causes additional spatial variability (the pancake structure) in the equatorial region, but it does not seem to greatly enhance the wave response.

[23] To further test these arguments, we perform an additional control simulation under solstitial conditions. The numerical experiment setup and the atmospheric conditions are identical to the control simulation of the solstice, and the only change is that the wave source is now moved to the summer hemisphere. Figure 7 shows the EPY and EPZ from this simulation, and it can be seen that the propagation of the wave energy is mainly upward with a branch crossing into the winter side and then deflected upward and back into the summer side, consistent with the waveguide. EPZ is much larger than the solstice case with the wave source in the winter hemisphere, and also larger than the pre-equinox EPZ below ~75 km above the wave source. It decrease rapidly when approaching the critical layer, and there is no sign of over-reflection from the unstable region. The wave amplitude of the zonal wind perturbation is similar to the amplitude in the pre-equinox case below ~75 km but much smaller above. The pancake structures is still present in the EP flux, but again it does not seem to affect the global wave response. By comparing the two control simulations at solstice, it is evident that at least two factors contribute to the weak 6.5-day wave response in the MLT region at solstice: (1) The strong eastward winter stratospheric jet is detrimental for the wave propagation from its source on the winter hemisphere; and (2) the "shielding" of the unstable region by the critical layer prevents wave over-reflection.

[24] Both observation [*Talaat et al.*, 2002] and our numerical simulation (e.g., Figure 2) show that the wave may become large again after equinox, with the wave amplitude larger on the early summer side. From the numerical simulation, it is also found the phase lines of the wave are much less tilted (almost vertical) below 80 km compared with those associated with the wave at pre-equinox. We know from Figure 3d that the curvature of the wind by day 120 in the summer mesosphere is already large enough so that $\bar{q}_\phi$ becomes negative in the polar mesosphere, while the winds in the stratosphere and mesosphere are still relatively small compared with the solstitial wind. From the analysis of the pre-equinox, equinox, and solstice cases, we expect that this wind condition be favorable for the wave propagation and amplification. This is confirmed by the EP flux plots for 6.5-day wave for day 113–125 in Figure 8. The main wave source is still located in the northern hemisphere, similar to

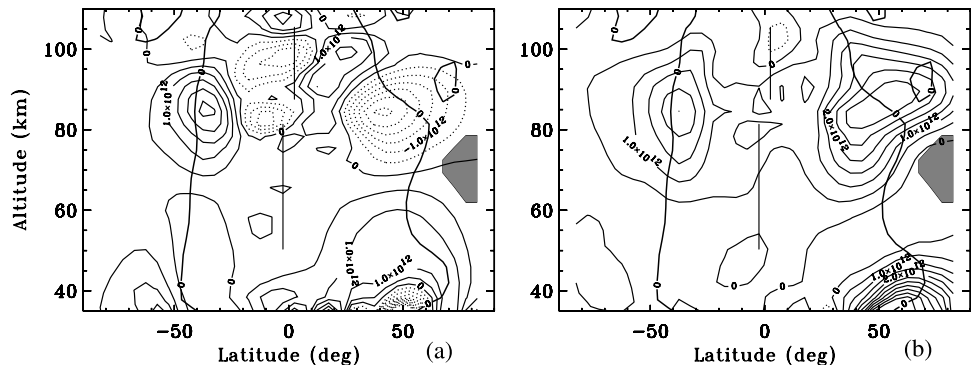

Figure 8. (a and b) Meridional and vertical components of the EP flux of the 6.5-day wave for the time period of day 113–125. The solid contours are for northward or upward directions. Both components have been normalized by the square root of the air density.

the pre-equinox case, but now in the same hemisphere as the unstable region. Below the unstable region, EP flux from the wave source is poleward and upward following the waveguide and away from the large eastward jet. The upward propagation of the wave energy below the unstable region is thus mainly confined to one hemisphere (early summer), which is different from the pre-equinox case. Strong enhancement of the wave activity can be seen from EPY and EPZ above the unstable region in both hemispheres. The wave also has a latitude structure similar to the first symmetric mode of a Rossby wave, again with the amplitude on the summer side larger. This explains the latitudinal shift of the 6.5-day wave peak around equinox from the late summer side to the early summer side (i.e., northward around March equinox and southward around September equinox). At the same time, the total EPY and EPZ decreases below the unstable region due to the superposition of the reflected and the original waves, and the phase lines of the superposed wave fields thus become less tilted.

3.3. Additional Variabilities

[25] From the analyses of these simulations, it is found that the 6.5-day wave is sensitive to the wind conditions. Hence the wave response at different seasons can be highly variable because of the wind variability. For example, at the fall equinox of this simulation, the curvature of the wind is quite large at middle to high latitudes of the southern mesosphere and there exists a pocket where $\bar{q}_\phi$ is negative. As a result, the wave is strongly enhanced in the mesosphere and lower thermosphere, as can be seen in Figures 1, 2a, and 2c.

[26] The winter stratosphere is warmer and the winter stratospheric jet is weaker at some years (for example, due to an ENSO event [e.g., *Sassi et al.*, 2004]), and the mean atmospheric conditions at solstice will be closer to the normal pre-equinoctial conditions as described above. The wave will then be more likely to propagate into the mesosphere. Furthermore, stratospheric sudden warming is more likely to occur earlier in the winter in such years, so that instability can be present in the winter mesosphere which can lead to wave amplification at a time when the wave is usually weak under ''normal'' conditions.

[27] In our numerical simulations, the perturbations are specified at ~10 hPa and we have focused on the wave propagation and global response in the MLT region. The sources of the wave also vary with time and latitude, as suggested by Figure 2d, but the variability of the wave in and below the stratosphere is beyond the scope of this study. We note that some results of our control simulations may be affected by this lower boundary. For example, the prescribed 6.5-day wave source has been confined to one hemisphere in the control simulations, which has implicitly assumed that there is no wave that has been ducted to the other hemisphere below 10 hPa. This is a fairly good approximation as indicated by the 1993 NCEP geopotential height perturbation (Figure 2d), but it may not be so in other years due to variability of the lower atmosphere. At solstice, if there is significant amount of wave being ducted to the summer hemisphere in the lower atmosphere, then we know from the control simulation that there can still be a large mesospheric response.

[28] Sensitivity tests have been performed by varying the forcing period (5 days and 7 days), under pre-equinoctial conditions with the wave source having the same latitudinal structure and amplitude as the one used in the control simulation for pre-equinox. In the simulation with 5-day wave forcing, the 5-day wave amplitude in the hemisphere opposite to the wave source is very weak (25–30%). The wave also amplifies above the unstable region, with the geopotential height amplitude at 62.5°S and 90 km twice as large as the amplitude at 75 km, a growth ratio similar to that of the 6.5-day wave. From the simulation results, there is no significant 6.5-day wave response to the 5-day wave forcing. Therefore the simulation result does not support the conjecture that the 6.5-day wave results from Doppler shift of the 5-day wave, at least under pre-equinoctial conditions. The distinction between the 5-day wave and the 6.5-day wave is also indicated by the difference in their interannual variability [*Miyoshi and Hirooka*, 2003]. In the simulation with 7-day wave forcing, the amplitude and the latitudinal structure of the 7-day wave response is similar to the 6.5-day wave below ~75 km. The wave amplification, however, is much weaker than the 6.5-day wave.

3.4. Discussions

[29] The quasi-two-day wave (QTDW) has zonal phase speed similar to that of a 6.5-day wave. As shown in HRDI observations [*Wu et al.*, 1993], the QTDW peaks in late January in the southern (summer) mesosphere. A plausible reason for this seasonal variation can be found by applying the same diagnostic tools as presented above to the QTDW. According to equation (1), the QTDW QG refractive index m is smaller with its larger zonal wave number (3) and more likely to become complex compared with 6.5-day wave under the same atmospheric conditions. The QTDW waveguide is thus more constrained to the lower latitudes and the seasonal span of the ''window'' period for its propagation is shorter than the 6.5-day wave. Figure 9 shows the diagnostic quantities for the mean atmosphere and QTDW on days 10, 30, 50, and 80, again calculated from the TIME-GCM/NCEP simulation of year 1993. Here the wave period has been chosen to be 2.17 days so that its phase speed is exactly the same as the 6.5-day wave. Compared with Figure 3, it is evident that the QTDW waveguide is more constrained in latitude, height, and time. Between day 10–30, the waveguide extends from the equatorial region at 10 hPa diagonally to 50–60° at the summer mesosphere and connecting to the region where $\bar{q}_\phi$ is negative. The waveguide shrinks afterward and moves away from the also shrinking negative $\bar{q}_\phi$ region. The waveguide disappears after day 60 and does not reappear until around June solstice. Therefore the QTDW may propagate into the mesosphere in the 2 months window period after solstice. Owing to the shielding by the critical layer, the wave may not be enhanced by the instability till later in this window period, i.e., from mid-January to early February.

[30] Figure 10 shows the meridional and vertical component of the QTDW (2.17-day) EP flux in a control simulation in this window period (day 30). In the simulation the wave source is still set in the winter hemisphere and its latitudinal distribution is similar to the control simulation for the 6.5-day wave at pre-equinox, with peak amplitude at 60°N. The wave energy propagation branches into two

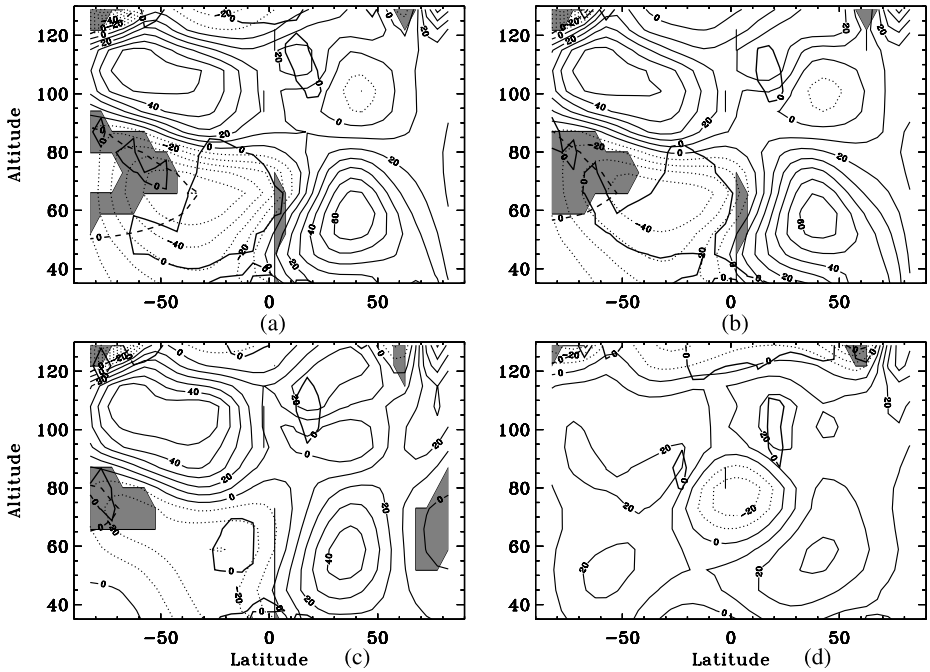

Figure 9. Similar to Figure 3 but for wave with wave number 3 and period of 2.17 days on days (a) 10, (b) 30, (c) 50, and (d) 80.

opposite latitudinal directions due to the winter jet. The equatorward branch shows little vertical propagation before reaching the waveguide. After crossing the equator and reaching the waveguide, the wave energy propagation follows the guide closely up into the mesosphere. Similar to the 6.5-day wave before and after equinox, over-reflection can be clearly seen from the increase of EPY and EPZ near the top of the unstable region. The poleward branch, on the other hand, does have a vertical component but decays rapidly with altitudes. Similar to the 6.5-day wave, the strongest enhancement of the wave is in the summer mesosphere. The latitudinal and height structure of the wave amplitude in the MLT (not shown) is similar to the amplitude structure of the fastest-growing Rossby-gravity mode with wave number 3 and period of about 2.1 days under solstitial conditions [*Salby and Callaghan*, 2001].

[31] From the analyses of the 6.5-day wave and QTDW, it is found that these waves may follow the waveguides and propagate from the lower atmosphere into the summer MLT in certain window periods between solstice and equinox. These waves may then over-reflect from the baroclinically/barotropically unstable region at middle to high latitudes in the mesosphere/mesopause and amplify by extracting energy from the mean flow. Therefore the variability at the middle and high latitudes in the summer MLT may closely track the variability in the lower atmosphere associated with these waves in these window periods. If the waves are strong, they may interact strongly with the mean flow in the MLT and modify the circulation, especially on the summer side. Figure 11 is the EP flux divergence (unit: ms^{-1} d^{-1}) of a strong 6.5-day wave, with maximum geopotential height perturbation of 300 m at 10 hPa, under pre-equinoctial

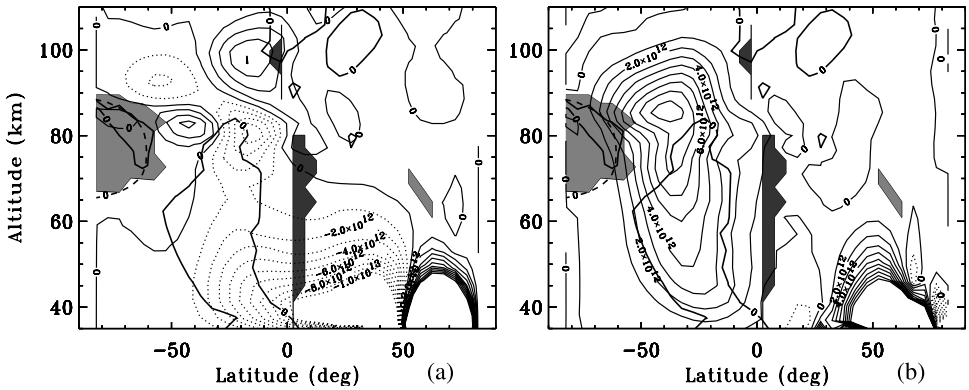

Figure 10. (a and b) Meridional and vertical components of the EP flux of the 2.17-day wave in the control simulation for day 30. The solid contours are for northward or upward directions. Both components have been normalized by the square root of the air density.

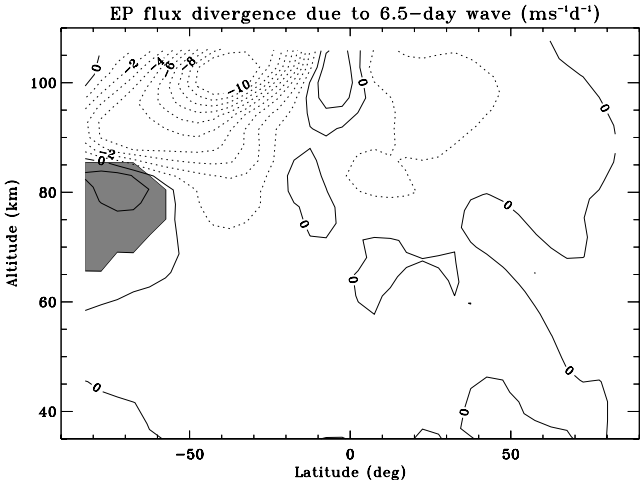

Figure 11. EP flux divergence ($ms^{-1}d^{-1}$) of the 6.5-day wave in the control simulation under pre-equinoctial conditions. The solid contours are for eastward forcing. The peak geopotential height perturbation of the 6.5-day wave source is 300 m and located at 60°N.

conditions. At the top of the unstable region (80–85 km), the divergence of the EP flux produces an eastward forcing of 1–2 ms^{-1} d^{-1}. The westward forcing above due to EP flux convergence reaches 10 $ms^{-1}d^{-1}$. The planetary wave forcing creates a poleward and downward circulation below ~90 km and poleward and upward circulation above, which in turn causes adiabatic heating and cooling, respectively. In the control experiment, there is a warming of about 3.5 K at 85 km and a cooling of similar magnitude at 100 km in the polar region. Therefore, if the lower winter hemisphere is more perturbed and planetary waves are stronger, it is likely that the summer MLT will be affected with a warmer summer mesosphere. This correlation has been identified by *Sassi et al.* [2004] for ENSO years.

4. Conclusions

[32] These simulations demonstrate the determining role of the atmospheric zonal wind in the propagation and amplification or decaying of the 6.5-day wave, and as the wind changes over the season, so does the wave. More specifically, the seasonal variability of the wave is closely dependent upon the variability of the waveguide, baroclinic/barotropic instability, and the critical layer of the wave, which are all determined by the wind.

[33] Before and after equinox, the wind condition is favorable for the wave propagation and amplification. This is because the wind is still relatively weak compared with solstice so that the wave may propagate without much decay. At the same time, the wind curvature is large enough in the summer mesosphere so that $\bar{q}_\phi$ becomes negative and the wave may amplify by extracting energy from the instability. This is further helped by the waveguide which extends into the high latitude summer mesosphere near the unstable region. The global response to the wave perturbation and amplification has a latitudinal structure similar to that of a first symmetric mode of a Rossby wave, though the amplitude is larger on the summer side due to the wave amplification by instability. The wave amplitude may also become large in the late winter mesosphere in a stratospheric sudden warming episode, when the winter jet reverses in the stratosphere and/or mesosphere and the $\bar{q}_\phi$ becomes negative. The detailed wave propagation and wave structure, however, can be different for the pre-equinox and postequinox periods because the location of the wave source can be different. Before equinox, the wave source is located on the late winter side, opposite to the unstable region in the late summer mesosphere, and its EP flux has a large cross equatorial component. The vertical component of the EP flux is shown to be large in both hemispheres, and the phase lines of the wave have a strong westward tilt. Shortly after equinox, on the other hand, the main wave source and the unstable region are on the same hemisphere at the early summer side. The wave propagation is mainly upward and confined to this side of the hemisphere, and the vertical component of the total EP flux is small due to the superposition of the original wave and the wave over-reflected from the unstable region. The phase lines of the wave is almost vertical at altitudes below the unstable region. At equinox, the zonal wind is generally weak and the atmosphere is stable. The wave can still propagate upward but without enhancement, and the wave amplitude is larger in the same hemisphere as the wave source. The large wave amplitude before and after equinox and the shift of the wave peak from the later summer side to the early summer side are consistent with observations.

[34] The 6.5-day wave amplitude in the mesosphere is small at solstice, even when the wave source (at ~10 hPa in the simulations) is comparable to or the same as those under other seasonal conditions. From the simulations, it is found that the wave decays significantly away from the wave source in both vertical and meridional directions due to the strong stratospheric winter jet. Further, the westward wind on the summer side is also strong and the latitudinal and height extension of the critical layer is so large that most of the unstable region is located poleward of the critical layer. The 6.5-day wave is thus prevented from reaching and amplifying at the unstable region. The inertial instability does not seem to affect the wave propagation and global wave response.

[35] Owing to the highly variable nature of the atmospheric zonal wind and the wave sources, the 6.5-day wave response in the MLT and its actual seasonal variability is also likely to vary. For example, the generally weaker winter stratospheric jet during ENSO is more favorable for the 6.5-day wave propagation. The amplification of the wave may also occur in the winter mesosphere during a stratospheric sudden warming (as seen in our simulation), when the stratospheric/mesospheric jet reversal is so large that the stratosphere/mesosphere becomes baroclinically/barotropically unstable.

[36] Sensitivity studies under pre-equinoctial conditions show that the 5-day wave response is very weak in the other hemisphere, while its amplification rate above the unstable region is similar to the 6.5-day wave. The 6.5-day wave response to the 5-day wave forcing is insignificant and no evidence is found that the 6.5-day wave results from Doppler shift of the 5-day wave. The 7-day wave is similar to the 6.5-day wave below the unstable region, but the wave amplification above is much weaker.

[37] Between solstice and equinox, there is also a period of time when the wave guide for the quasi-two-day wave extends from the lower atmosphere to the summer mesosphere, close to the baroclinically/barotropically unstable region. As the 6.5-day wave, the QTDW can propagate from the lower atmosphere into the mesosphere and amplify above the unstable region within this window period. The global structure of the wave in the MLT from the simulation is very similar to that obtained from the generalized normal mode calculation [*Salby and Callaghan*, 2001]. Both the spatial extent and temporal span of the waveguide, however, is more constrained compared with the 6.5-day wave. This is because QTDW has phase speeds similar to those of the 6.5-day wave but larger zonal wave number so that the refractive index of the wave is smaller and more likely to become complex. Also similar to the 6.5-day wave, the QTDW is likely to be prevented from reaching and amplifying at the unstable region by the critical layer at solstice. This provides a plausible explanation to the observation that the QTDW peaks in the summer mesosphere in late January.

[38] Because of the waveguides for 6.5-day wave and QTDW extending from the lower atmosphere to the summer mesosphere and the baroclinic/barotropic instability at the summer mesosphere, the variability in the summer MLT may closely track the lower atmospheric variability associated with these waves during the window periods. The amplified wave above the unstable region may interact strongly with the mean circulation in the summer MLT. Such interaction may be especially strong during ENSO years.

[39] **Acknowledgments.** We thank F. Sassi and two anonymous reviewers for their helpful comments. HLL's effort is in part supported by the NASA Sun Earth Connection Theory Program (S-13753-G). The National Center for Atmospheric Research is sponsored by National Science Foundation.

References

Andrews, D. G., J. R. Holton, and C. B. Leovy (1987), *Middle Atmosphere Dynamics*, 489 pp., Academic, San Diego, Calif.

Charney, J. G., and P. G. Drazin (1961), Propagation of planetary scale disturbances from the lower to the upper atmosphere, *J. Geophys. Res.*, *66*, 83–109.

Dickinson, R. E., E. C. Ridley, and R. G. Roble (1981), A three-dimensional general circulation model of the thermosphere, *J. Geophys. Res.*, *86*, 1499–1512.

Dickinson, R. E., E. C. Ridley, and R. G. Roble (1984), Thermospheric general circulation with coupled dynamics and composition, *J. Atmos. Sci.*, *41*, 205–219.

Geisler, J. E., and R. E. Dickinson (1976), The 5-day wave on a sphere with realistic zonal winds, *J. Atmos. Sci.*, *33*, 632–641.

Hagan, M. E., and R. G. Roble (2001), Modeling diurnal tidal variability with the national center for atmospheric research thermosphere-ionosphere-mesosphere-electrodynamics general circulation model, *J. Geophys. Res.*, *106*, 24,869–24,882.

Hagan, M. E., J. M. Forbes, and F. Vial (1995), On modeling migrating solar tides, *Geophys. Res. Lett.*, *22*, 893–896.

Hagan, M. E., M. D. Burrage, J. M. Forbes, J. Hackney, W. J. Randel, and X. Zhang (1999), GSWM-98: Results for migrating solar tides, *J. Geophys. Res.*, *104*, 6813–6828.

Hirota, I., and T. Hirooka (1984), Normal mode Rossby waves observed in the upper stratosphere, part 1: First symmetric modes of zonal wavenumbers 1 and 2, *J. Atmos. Sci.*, *41*, 1253–1267.

Lieberman, R. S., D. M. Riggin, S. J. Franke, A. H. Manson, C. Meek, T. Nakamura, T. Tsuda, R. A. Vincent, and I. Reid (2003), The 6.5-day wave in the mesosphere and lower thermosphere: Evidence for baroclinic/barotropic instability, *J. Geophys. Res.*, *108*(D20), 4640, doi:10.1029/2002JD003349.

Limpasuvan, V., C. B. Leovy, Y. J. Orsolini, and B. A. Boville (2000), A numerical simulation of the two-day wave near the stratopause, *J. Atmos. Sci.*, *57*, 1702–1717.

Lindzen, R. S. (1981), Turbulence and stress owing to gravity wave and tidal breakdown, *J. Geophys. Res.*, *86*, 9707–9714.

Madden, R. A., and P. A. Julian (1972), Further evidence of global-scale 5-day pressure waves, *J. Atmos. Sci.*, *29*, 1464–1469.

Meyer, C. K., and J. M. Forbes (1997), A 6.5-day westward propagating planetary wave: Origin and characteristics, *J. Geophys. Res.*, *102*, 26,173–26,178.

Miyoshi, Y., and T. Hirooka (2003), Quasi-biennial variation of the 5-day wave in the stratosphere, *J. Geophys. Res.*, *108*(D19), 4620, doi:10.1029/2002JD003145.

Richmond, A. D., E. C. Ridley, and R. G. Roble (1992), A thermosphere/ionosphere general circulation model with coupled electrodynamics, *Geophys. Res. Lett.*, *19*, 601–604.

Riggin, D. M., D. C. Fritts, T. Tsuda, T. Nakamura, and R. A. Vincent (1997), Radar observations of a 3-day kelvin wave in the equatorial mesosphere, *J. Geophys. Res.*, *102*, 26,141–26,158.

Roble, R. G. (1995), Energetics of the mesosphere and thermosphere, in *The Upper Mesosphere and Lower Thermosphere: A Review of Experiment and Theory*, *Geophys. Monogr. Ser.*, vol. 87, edited by R. M. Johnson and T. L. Killeen, pp. 1–22, AGU, Washington, D. C.

Roble, R. G., and E. C. Ridley (1994), A thermosphere-ionosphere-mesosphere-electrodynamics general circulation model (TIME-GCM): Equinox solar cycle minimum simulations (30–500 km), *Geophys. Res. Lett.*, *21*, 417–420.

Roble, R. G., E. C. Ridley, and R. E. Dickinson (1987), On the global mean structure of the thermosphere, *J. Geophys. Res.*, *92*, 8745–8758.

Roble, R. G., E. C. Ridley, A. D. Richmond, and R. E. Dickinson (1988), A coupled thermosphere/ionosphere general circulation model, *Geophys. Res. Lett.*, *15*, 1325–1328.

Salby, M. L. (1997), *Fundamentals of Atmospheric Physics*, 627 pp., Academic, San Diego, Calif.

Salby, M. L., and P. F. Callaghan (2001), Seasonal amplification of the 2-day wave: Relationship between normal mode and instability, *J. Atmos. Sci.*, *58*, 1858–1869.

Sassi, F., R. R. Garcia, and B. A. Boville (1993), The stratopause semi-annual oscillation in the NCAR Community Climate Model, *J. Atmos. Sci.*, *50*, 3608–3624.

Sassi, F., D. Kinnison, B. A. Boville, R. R. Garcia, and R. G. Roble (2004), Effect of El Nino–Southern Oscillation on the dynamical, thermal, and chemical structure of the middle atmosphere, *J. Geophys. Res.*, *109*, D17108, doi:10.1029/2003JD004434.

Talaat, E. R., J. H. Yee, and X. Zhu (2001), Observations of the 6.5-day wave in the mesosphere and lower thermosphere, *J. Geophys. Res.*, *106*, 20,715–20,723.

Talaat, E. R., J.-H. Yee, and X. Zhu (2002), The 6.5-day wave in the tropical stratosphere and mesosphere, *J. Geophys. Res.*, *107*(D12), 4133, doi:10.1029/2001JD000822.

Torrence, C., and G. P. Compo (1998), A practical guide to wavelet analysis, *Bull. Am. Meteorol. Soc.*, *79*, 61–78.

Walterscheid, R. L., G. G. Sivjee, and R. G. Roble (2000), Mesospheric and lower thermospheric manifestation of a stratospheric warming event over Eureka, Canada (80°N), *Geophys. Res. Lett.*, *27*, 2897–2900.

Wu, D. L., P. B. Hays, W. R. Skinner, A. R. Marshall, M. D. Burrage, R. S. Lieberman, and D. A. Ortland (1993), Observations of the quasi 2-day wave from the high-resolution doppler imager on UARS, *Geophys. Res. Lett.*, *20*, 2853–2856.

Wu, D. L., P. B. Hays, and W. R. Skinner (1994), Observations of the 5-day wave in the mesosphere and lower thermosphere, *Geophys. Res. Lett.*, *21*, 2733–2736.

R. S. Lieberman and D. M. Riggin, Colorado Research Associates Division, NorthWest Research Associates, Inc., 3380 Mitchell Lane, Boulder, CO 80301, USA. (ruth@colorado-research.com; riggin@colorado-research.com)

H.-L. Liu and R. G. Roble, High Altitude Observatory, National Center for Atmospheric Research, Boulder, CO 80307-3000, USA. (liuh@ucar.edu; roble@ucar.edu)

E. R. Talaat and J.-H. Yee, Johns Hopkins University, Applied Physics Laboratory, 11100 Johns Hopkins Road, Laurel, MD 20723-6099, USA. (elsayed.talaat@jhuapl.edu; sam.yee@jhuapl.edu)